



ACADEMIC
PRESS

Available online at www.sciencedirect.com

SCIENCE @ DIRECT®

NeuroImage

NeuroImage 20 (2003) 752–764

www.elsevier.com/locate/ynimg

Electrical impedance tomography of human brain function using reconstruction algorithms based on the finite element method

Andrew P. Bagshaw,^{a,1} Adam D. Liston,^b Richard H. Bayford,^b Andrew Tizzard,^b
Adam P. Gibson,^c A. Thomas Tidswell,^a Matthew K. Sparkes,^a Hamid Dehghani,^d
Colin D. Binne,^e and David S. Holder^{a,*}

^a Department of Clinical Neurophysiology, University College London, UK

^b School of Health and Social Sciences, Middlesex University, London, UK

^c Department of Medical Physics and Bioengineering, University College London, UK

^d Thayer School of Engineering, Dartmouth College, Hanover, NH 03755, USA

^e Department of Clinical Neurophysiology, Kings College Hospital, London, UK

Received 22 July 2002; revised 17 April 2003; accepted 1 May 2003

Abstract

Electrical impedance tomography (EIT) is a recently developed technique which enables the internal conductivity of an object to be imaged using rings of external electrodes. In a recent study, EIT during cortical evoked responses showed encouraging changes in the raw impedance measurements, but reconstructed images were noisy. A simplified reconstruction algorithm was used which modelled the head as a homogeneous sphere. In the current study, the development and validation of an improved reconstruction algorithm are described in which realistic geometry and conductivity distributions have been incorporated using the finite element method. Data from computer simulations and spherical or head-shaped saline-filled tank phantoms, in which the skull was represented by a concentric shell of plaster of Paris or a real human skull, have been reconstructed into images. There were significant improvements in image quality as a result of the incorporation of accurate geometry and extracerebral layers in the reconstruction algorithm. Image quality, assessed by blinded subjective expert observers, also improved significantly when data from the previous evoked response study were reanalysed with the new algorithm. In preliminary images collected during epileptic seizures, the new algorithm generated EIT conductivity changes which were consistent with the electrographic ictal activity. Incorporation of realistic geometry and conductivity into the reconstruction algorithm significantly improves the quality of EIT images and lends encouragement to the belief that EIT may provide a low-cost, portable functional neuroimaging system in the foreseeable future.

© 2003 Elsevier Inc. All rights reserved.

Introduction

Electrical impedance tomography (EIT) is a noninvasive technique whereby images of the conductivity within a body can be reconstructed from voltage measurements made on the surface (Webster, 1990; Boone et al., 1997). Electrodes are attached to the body in a similar fashion to electroencephalography (EEG), and each measurement is typically

made from a combination of four electrodes, two to inject current and two to sample the resulting voltage distribution. For a particular pair of current injection electrodes, several voltage measurements are taken, the injection pair is then switched, and the process repeated to produce one complete data set. A reconstruction algorithm is used to relate the measured voltages to the conductivity within the body (Barber and Seagar, 1987; Metherall et al., 1996). EIT has been applied to imaging of the thorax and abdomen, particularly where there is a conductivity change between passive and active states, for example when measuring gastric function following a saline drink (Mangall et al., 1987) or during ventilation (Harris et al., 1988; Serrano et al., 2002), and has

* Corresponding author. Department of Clinical Neurophysiology, Middlesex Hospital, Mortimer Street, London W1T 8AA, UK.

¹ Current address: Montreal Neurological Institute, McGill University, Montréal, Québec H3A 2B4, Canada.

also been used in breast imaging (Osterman et al., 2000; Cherepenin et al., 2001).

Recently, EIT has been applied to the problem of functional imaging in the human brain (Gibson, 2000; Towers et al., 2000; Tidswell et al., 2001a), where conductivity increases and decreases can occur as a result of changes in blood volume, as blood has a higher conductivity than the surrounding tissue (Geddes and Baker, 1967). Conductivity decreases can also be caused by cell swelling (Lux et al., 1986).

In one study (Tidswell et al., 2001a), measurements were taken from human volunteers performing visual, motor, and somatosensory tasks using 31 electrodes applied to the scalp in the same way as in EEG, in the standard 10–20 configuration (Binnie et al., 1982). Two hundred and fifty eight individual voltage measurements were taken to produce one data set. Changes of the order of 0.5–1.0% were observed in the raw voltage data during visual-evoked responses in healthy volunteers. This is consistent with previous work with EIT using electrodes placed on the exposed cortex of anaesthetised rabbits, which showed that the magnitude of the conductivity changes during evoked responses was about 5% and during an induced epileptic seizure, about 10% (Holder et al., 1996; Rao, 2000). By the time the signal has been attenuated by the skull, the magnitude of scalp measurements is of the order of 10 times smaller than cortical measurements. Although reproducible voltage changes were evident in the raw data in 51 out of 52 recordings, only 19 of the reconstructed image sets demonstrated a significant conductivity change with reasonable anatomical localisation. As the resolution and localisation accuracy of EIT images are relatively poor, reasonable localisation for visual stimuli was defined as a conductivity increase, corresponding to a blood volume increase, in the posterior quadrant of the image. Similarly, conductivity increases in the contralateral hemisphere were considered to be acceptable for motor stimuli. One possible explanation for the discrepancy between the raw data and the images is that significant errors were introduced into the image reconstruction process because the head was modelled as a sphere of uniform conductivity.

The image reconstruction process can be divided into two parts. A forward model is used to predict the current flow and hence the scalp voltage measurements that will occur for a particular internal conductivity distribution and current injection protocol. Ideally, the forward model would give an accurate representation of the geometry of the human head and be capable of incorporating the conductivities and anisotropies of the various regions, such as the scalp, skull, cerebro-spinal fluid (CSF), white and grey matter of the brain, as well as discontinuities in the skull, such as the sutures and the eye sockets (van den Broek et al., 1998). This is a complex problem computationally, and some degree of simplification is required, whether it is to assume that the problem is two dimensional (Tarassenko, 1985; Gibson et al., 2000; Tidswell et al., 2001c) or, if three

dimensional, that the head has a simplified geometry (Towers et al., 2000; Bonovas et al., 2001; Tidswell et al., 2001a, 2001b). If the geometry is simple, such as a sphere, the current flow and voltage distribution throughout the volume can be calculated analytically. When the geometry is more complex, no analytical solution exists and a numerical method such as the finite element method (FEM) must be used (e.g., Burnett, 1987; Jin, 1993). In this case, the volume is divided into many small elements of known shape, such as tetrahedra, and the potential is calculated within each element to give the distribution throughout the whole volume. Numerical approaches tend to be more general and allow not only realistic geometry to be included in the forward model, but also anisotropy and discontinuities. However, even with this method there are severe technical difficulties in producing an anatomically accurate model that will allow stable and accurate solutions to be calculated.

The second part of the reconstruction process is the inverse solution. The information from the forward model, which gives the scalp voltage measurements that are expected for a conductivity change within the brain, is used in the inverse solution to produce an approximate internal conductivity distribution from a measured set of boundary voltages. In difference imaging, changes in the internal conductivity distribution are reconstructed from changes in boundary voltages. This is in contrast to static imaging where a map of absolute conductivity values is constructed from voltage measurements taken at a single point in time. Difference imaging, which is the technique used in this work, is much more forgiving of inaccuracies in the forward model. The relationship between the measured boundary voltages and the internal conductivity, as determined by the forward model, can be expressed in the form of a sensitivity matrix. The reconstruction algorithm used by Tidswell et al. (2001a) used a sensitivity matrix which assumed that the human head was a homogeneous sphere, an assumption that contains a number of unquantified errors, and it was not clear to what extent inaccuracies in the forward model were responsible for the localisation failures.

This type of question has been addressed in the field of EEG and magnetoencephalography (MEG) inverse dipole localisation and significant improvements in localisation accuracy have been noted when a more accurate forward model is used (e.g., Roth et al., 1993; Menninghaus et al., 1994; Yvert et al., 1997; Crouzeix et al., 1999; Huiskamp et al., 1999; Cuffin, 2001; Cuffin et al., 2001). For example, Roth et al. (1993) generated potential distributions using a realistically shaped forward model, and performed the inverse solution using a three-shell spherical model. In the temporal and frontal regions the localisation error was as large as 4 cm when using the spherical model. Physically, the EIT problem is similar to the EEG problem, which suggests that significant improvements in the ability of EIT to localise conductivity changes within the brain may be possible if a more realistic forward model is used.

The purpose of this paper is to present a validated re-

construction algorithm for EIT of human brain function which uses the finite element method to incorporate realistic geometry and conductivities in the forward model. The implementation of the FEM itself has been validated by comparison with analytical solutions for a homogeneous sphere.

The intention of the work was to answer three questions: What is the advantage of using realistic, head-shaped geometry? What is the advantage of having shells of different conductivities? How much difference does this make to images reconstructed from human data?

The first two questions were addressed separately using simulated data and data collected from saline-filled tank phantoms, designed to simulate the shape and structure of the forward models. By producing images using an algorithm based on an accurate forward model, for example, containing realistic geometry or shelled conductivities, and comparing them with images produced using a homogeneous sphere forward model, insight can be gained into the importance of the aspect of the forward model under consideration.

Once the effect of incorporating realistic geometry and realistic conductivities into the forward model had been assessed, the final question was addressed. Data were collected from human volunteers performing motor and visual tasks and images produced using a sensitivity matrix for a realistic head model, and one for a homogeneous sphere forward model. At the present stage, only a few examples are given from data previously presented by Tidswell et al. (2001a). Finally, images will be presented from a pilot study into one of the principal clinical applications of a working EIT system, namely the localisation of the foci of epileptic seizures from data collected ictally. Data from four seizures in two patients were reconstructed using the sensitivity matrix for the realistic head, and the position of any localised conductivity changes compared with EEG telemetry data.

Materials and methods

EIT image reconstruction

The problem in EIT image reconstruction is to calculate an internal conductivity map from measurements made on the surface of the object. In general, the measured potential is a nonlinear function of conductivity. However, the conductivity changes that are expected in the brain are sufficiently small (less than 20% (Holder et al., 1996)) that, when images of changes in conductivity are being produced from changes in the boundary voltages, it can be assumed that the relationship between potential and conductivity is linear. This approach has been adopted in the current work.

The forward model can be used to calculate a sensitivity matrix A which links the change of each surface impedance measurement, ΔV , to the change in conductivity of each

pixel, $\Delta\sigma$ (Eq. (1)). The sensitivity at a given point is proportional to the scalar product of the electric fields which would exist if each pair of electrodes was made to inject current (Geselowitz, 1971; Murai and Kagawa, 1985). Different sensitivity matrices can be produced using different forward models to calculate the potential distribution within the object, as given by Laplace's equation.

$$\Delta V = A \Delta\sigma \quad (1)$$

$$\Delta\sigma = A^\dagger \Delta V \quad (2)$$

The sensitivity matrix is then inverted to give the pseudo inverse A^\dagger which is multiplied by the measured voltages to give an image of conductivity change (Eq. (2)).

The sensitivity matrix is ill-conditioned, so must be regularised before it can be inverted. Many different regularisation techniques have been used in EIT (see Vauhkonen, 1997, for a review), but in this work the sensitivity matrix was inverted using truncated singular value decomposition (SVD) (Zadachkoochak et al., 1991; Golub and Loam, 1996; Xu, 1998; Kleiner mann, 2001). It was found that normalisation of the sensitivity matrices based on spherical and homogeneous forward models prior to inversion improved the resulting images (Barber and Seager, 1987; Kotre, 1994), but introduced artefacts into the images reconstructed using the sensitivity matrix based on the full shelled head forward model. The reason for this is unclear and requires further investigation. The sensitivity matrix based on the full shelled head used in this work was not normalised.

The truncation singular value was 70 in all cases. This value was chosen as it gave good localisation accuracy for the data from the head-shaped tank, without the skull. Although this may mean that the truncation level is not optimal, the fact that the sensitivity matrices are very similarly conditioned (the 70th singular value has a contribution of 0.0013 to 0.004 of the maximum singular value for all the matrices used) means that the errors introduced are similar for the different matrices. Difference imaging is also relatively robust to the number of singular values included in the reconstruction (Gibson, 2000), suggesting that the method employed here is adequate for the purpose of comparing the different sensitivity matrices. An optimum truncation level for each sensitivity matrix can be determined using a number of more sophisticated methods (Hansen, 1998; Xu, 1998).

Numerical solutions using the finite element method

All of the finite element meshes used in the current work were generated using I-DEAS (EDS, MO), a commercial software package designed primarily for use in stress and thermal modelling. The suitability of I-DEAS for mesh generation and the possibility of solving the forward problem in EIT of the human head have been considered previously (Bayford et al., 2001). In the

present case, I-DEAS was used purely to generate the meshes, and not as a solver. The mesh generation is based on an advancing front algorithm. All meshes were constructed from linear, tetrahedral elements.

The homogeneous and four-shell spherical meshes had an outer radius of 92 mm (Fig. 1a and b). The four shells had outer radii (conductivities) of 80 mm (0.25 S m^{-1}) for the brain, 82 mm (1.79 S m^{-1}) for the CSF, 87 mm (0.018 S m^{-1}) for the skull, and 92 mm (0.44 S m^{-1}) for the scalp (Burger and Milaan, 1943; Geddes and Baker, 1967; Baumann et al., 1997). The conductivity of the skull is that measured recently by Oostendorp et al. (2001), which is significantly higher than the value of Law (1993).

The head-shaped meshes were produced using a solid model generated using nonuniform rational B-spline (NURB) surfaces of the head, skull, CSF and brain (Fig. 1c and 2). The main head form was produced by lofting a series of NURB curves that were fitted to a segmented MRI. The skull also used segmented MRI section data as a basis for the form but these proved inadequate in themselves for generating accurate surfaces for the jaw, eye socket, and nasal cavity geometry. Additional data in the form of photographs of anatomical models and reconstructed images from the Visible Human Project were cast as image planes for surface modelling (www.nlm.nih.gov/research/visible/visible_human.html). These data also enabled more realistic modelling of the brain and spinal column to be carried out, as well as some idealised representation of vertebrate from C1 to C3.

The electric field was calculated at each node in the mesh using a linear finite element solver written in Matlab (The MathWorks Inc., MA). The sensitivity at each node was calculated using Geselowitz's theorem (Geselowitz, 1971; Deghani, 1999). The sensitivity matrix was created by performing the calculation for each node in the mesh and for all combinations of current injection and voltage measurement electrodes. In all cases, point electrodes were assumed, located at the node closest to the actual position of each electrode.

Analytical solution for a homogeneous sphere

A sensitivity matrix was generated based on an analytical solution for a homogeneous sphere to determine the accuracy of the numerical solutions. The interior potential for the homogeneous sphere was derived from the Neumann solution (Kevorkian, 1990; Gibson, 2000). The sensitivity at each node was calculated from the potential in the same way as for the numerical solutions.

Method of comparing forward solutions

The accuracy of the FEM implementation was assessed by comparing the potentials generated at the electrodes with those generated by an analytical solution. Comparisons

were made between the analytical solution and the finite element solution calculated on spherical meshes of different nodal density. The analytical boundary voltages were calculated at the coordinates of the nodes used as the point electrodes for each mesh. The error for each mesh was defined as the maximum difference between the numerical and the analytical boundary voltages divided by the maximum (analytical) voltage (Jain et al., 1997).

Generation of simulated data

Two sets of simulated data were generated. One used a forward model which incorporated realistic geometry, but which had homogeneous conductivity, the other used a forward model which had spherical shape, but which contained four shells with conductivities appropriate for the brain, CSF, skull, and scalp. These data were then reconstructed into images assuming either the correct forward model (that is, either a homogeneous head or a four shelled sphere), or a forward model based on a homogeneous sphere. The meshes used to generate the data were different from those used to reconstruct it. For example, a fine homogeneous head-shaped mesh was used to generate data, and solutions from a coarser mesh were used in the reconstruction process.

Boundary voltages were generated for a conductivity distribution which included a 1-cm-radius spherical conductivity increase of 20% in the brain region, at 15 positions at 10-mm intervals along the y axis (anterior-posterior). The boundary voltages were expressed relative to the equivalent boundary voltages calculated without the inhomogeneity present (as in Eq. (1)), and these data were reconstructed.

Tank phantom construction

A spherical tank of diameter 187 mm was constructed consisting of two hemispherical shells of Perspex bolted together across a rubber seal (Fig. 3a). Silver ball electrodes were placed on the inside of the sphere in the 10–20 configuration (Binnie et al., 1982). Within the sphere, to simulate the skull, was a spherical shell cast in dental grade plaster of Paris (calcium sulphate hexahydrate, Vel-Mix Stone, Kerr Ltd, UK). The tank was filled with a saturated solution of calcium sulphate to prevent the simulated skull from dissolving. The solution had a conductivity of 0.25 S m^{-1} , similar to that of brain tissue, and the skull was mixed in such a ratio that its conductivity was 0.012 S m^{-1} when soaked in the solution. The resistivity ratio of the shell to its surroundings was therefore about 21:1, which lies between that reported by Oostendorp et al. (2000) and measurements by Saha and Williams (1992) and Geddes and Baker (1967).

A realistically head-shaped tank was constructed from a silicone rubber cast of a head-shaped model made from a human skull covered with clay. Thirty one Ag/AgCl electrodes of 1 cm diameter were embedded into the inner walls of the tank during the casting process (Fig. 3b). The tank was filled with 0.2% saline to represent the brain (Tidswell et al., 2001b).

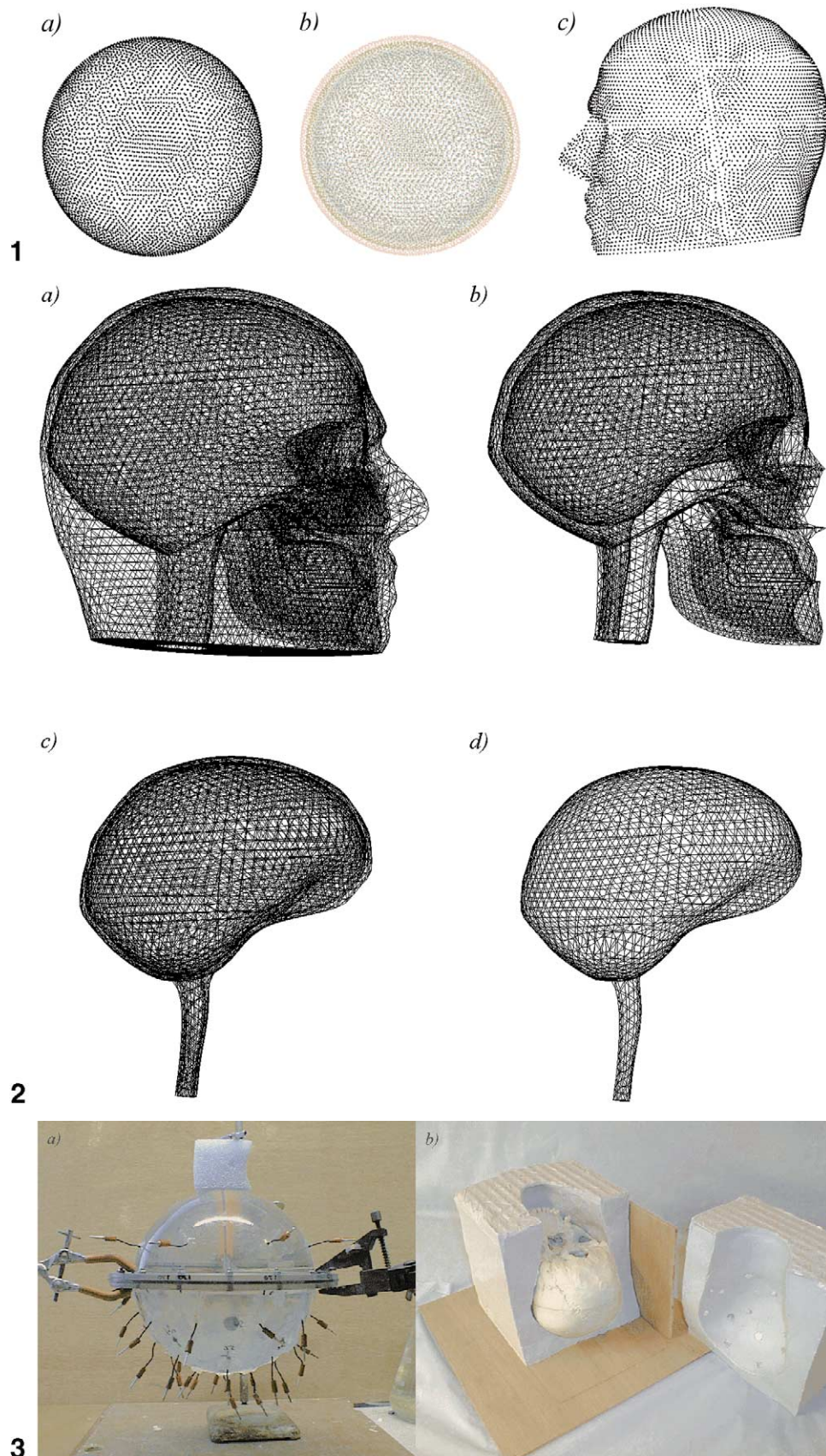


Fig. 1. The nodes on the surfaces of (a) the homogeneous spherical mesh with 24734 nodes and 130229 elements, (b) the four-shell mesh with 26934 nodes and 146363 elements, and (c) the homogeneous head-shaped mesh with 22420 nodes and 106825 elements. In (b) the nodes on each surface of the four shells are shown. Fig. 2. The element faces on the surfaces of the four parts of the full shelled head mesh: (a) the scalp, (b) the skull, (c) the CSF, and (d) the brain region. The scalp region contains 8067 nodes, the skull region 6122 nodes, the CSF region 2018 nodes, and the brain region 3566 nodes. Fig. 3. (a) The spherical tank phantom, shown for clarity without the presence of the shell to represent the skull and (b) the head-shaped tank phantom shown with the two halves separated and a human skull inside.

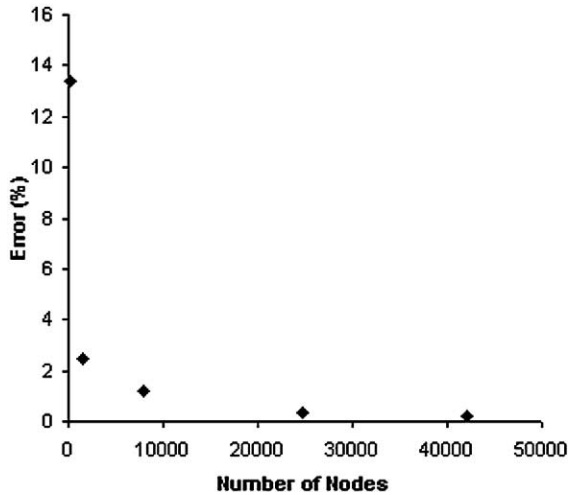


Fig. 4. The error in the numerical boundary voltages for the homogeneous spherical meshes, compared with the analytical solution.

Data were collected from this tank both with and without the presence of a human skull in order to investigate the effect of shape alone, and the combined effect of shape and layers of different conductivities. The resistivity ratio between the skull and the brain region was approximately 98:1 (Tidswell et al., 2001b). This is higher than in the human head and represents a more stringent test for the reconstruction process.

Generation of tank phantom data

The process that was followed for the simulated data was repeated with data collected from tanks. Data from a homogeneous head-shaped tank were reconstructed assuming both correct (head-shaped) forward geometry and spherical forward geometry. Similarly, data from a shelled spherical tank were reconstructed with correct and homogeneous forward conductivity distributions. Finally, data collected from a head-shaped tank incorporating a real human skull were reconstructed with a shelled head-shaped forward model, and these images were compared with those produced assuming a homogeneous sphere as the forward model (Table 1).

Through a hole at the top of the spherical tank (Fig. 3a), a 1-mm-diameter wooden support was inserted in order to suspend a 6.3-cm³ cylinder of Perspex (length 2 cm, diameter 2 cm) at 11 positions along the y axis. For each position, image data sets were acquired for a period of 210 s. The support was present throughout and was used to hold the Perspex for 40 s of stimulus during this time.

As the spherical tank contained only three shells, a sensitivity matrix was also created using a forward model based on three concentric shells, representing the brain, skull, and scalp, by modifying the conductivity of the nodes in the CSF of the four-shell mesh, and designating them as brain nodes. The conductivities of the brain and scalp were both set to 0.25 S m⁻¹, and the skull to 0.012 S m⁻¹ in accordance with the measured conductivities of the plaster of Paris skull and the bathing solution.

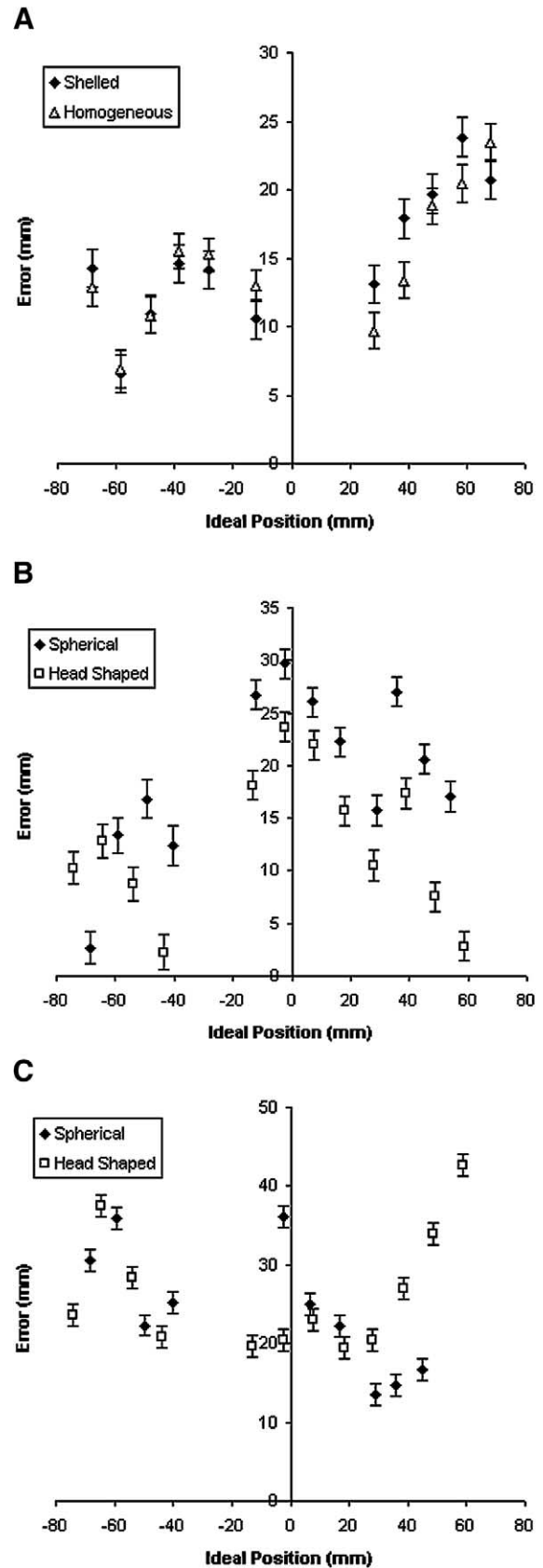


Fig. 5. Localisation error for the images produced from tank phantom data: (a) shelled spherical tank data reconstructed with A_{3shell} and A_{sphere} , (b) homogeneous head tank data reconstructed with $A_{homhead}$ and A_{sphere} , and (c) data from the head tank with skull, reconstructed with $A_{shellhead}$ and A_{sphere} .

Table 1
A summary of the purpose of the tank phantom studies

Source of data	Reconstruction method	Sensitivity matrix notation	Purpose
Three-shell spherical tank	Shelled	$A_{3\text{Shell}}$	Investigate effect of shells
	Homogeneous	A_{sphere}	
Homogeneous head tank	Head shaped	A_{homhead}	Investigate effect of realistic geometry
	Spherical	A_{sphere}	
Head with skull tank	Head shaped	$A_{\text{shellhead}}$	Investigate effect of both realistic geometry and shells
	Spherical	A_{sphere}	

In the head-shaped tank (Fig. 3b), both with and without the skull, data were collected with the Perspex cylinder at 12 positions along the anterior-posterior line. The data from the head-shaped tank with a skull were collected using an EIT system which incorporates an HP 4282A impedance analyser (Tidswell et al., 2001a). All of the other tank data were collected using the UCLH Mark 1b EIT system at 38 kHz (Yerworth et al., 2002).

Method of comparing reconstructed images

The parameters that were used to compare the reconstructed image were the localisation accuracy, the resolution, and the image quality. The localisation error was defined as the distance between the peak of the conductivity change in the image and the real position in either the simulated data or the tank phantom. The resolution was defined as the half-width at half-maximum (HWHM), measured along the anterior-posterior axis (y axis) in the plane normal to the superior-inferior axis (z axis) at which the maximum conductivity change occurred.

In addition to these two quantitative measures, two observers (DSH and ATT) performed a semiblinded assessment of the image quality. Each image was marked on a scale of 1 (poor quality) to 10 (excellent quality). The assessors were told the approximate position of the expected conductivity change, and whether the reconstructed data were from a tank or human volunteers. They were not told which sensitivity matrix had been used to reconstruct the images, although the shape of the image allowed them to distinguish between reconstructions based on spherical or head-shaped forward models. The assessors took into account the correctness of the localisation from their knowledge of the ideal position of the conductivity change, and the level of noise in the image. For the images reconstructed from tank data, a mark was given for each position of the Perspex. For the images reconstructed from human data, a single mark was given.

On the colour scale used in the images (Fig. 6 to 10), an increase in conductivity is shown as darker (blue) colours, while a decrease in conductivity is shown by lighter (red) colours. No change in conductivity with respect to the reference is denoted by black. The $z = 0$ plane is defined by the EEG 10–20 electrodes Fp1, Fp2, T3, T4, O1, and O2. The front of the head is at the top of the image, and the left hand side of the image corresponds to the left hand side of the head.

Human data—Visual and motor stimuli

Data are presented from two volunteers performing a visual task (observation of an 8 Hz chequerboard at a distance of 30 cm), and from two volunteers performing a motor task (self-paced, sequential apposition of the thumb and fingers, one of the left hand and one of the right hand). In each case, a baseline reading was taken for 150 s, followed by stimulus for 75 s and then recovery for a further 150 s.

The data are selected from those presented previously by Tidswell et al. (2001a) on the basis that a conductivity increase with reasonably accurate localisation was present in the images reconstructed with the sensitivity matrix based on the full shelled head forward model. Comparison is made with the images produced by reconstructing the same data with the sensitivity matrix based on the homogeneous sphere forward model. The data are the average of five repeated measurements and the images have been thresholded so that only changes that are two standard errors above the mean background noise are shown.

Human data—Ictal

Images are presented from data collected from two patients during complex partial seizures. EEG telemetry data were collected simultaneously with the EIT data acquisition. Patient 1 was a 32-year-old male with a left dysembryoplastic neuroepithelial tumour (DNET). EEG telemetry data show bilateral ictal activity which is maximal at the right anterior temporal electrode. Patient 2 was a 20-year-old male with left hippocampal atrophy. The EEG shows occasional left spikes interictally, with left ictal activity with secondary generalisation. In each case, the reconstructed data are the result of averaging 10 sets of 258 individual voltage measurements, or approximately 3 s worth of data.

Results

Comparison of forward solutions

The potentials calculated numerically for a homogeneous sphere agree with those calculated analytically to within 0.5% for meshes containing 20,000 nodes or more (Fig. 4).

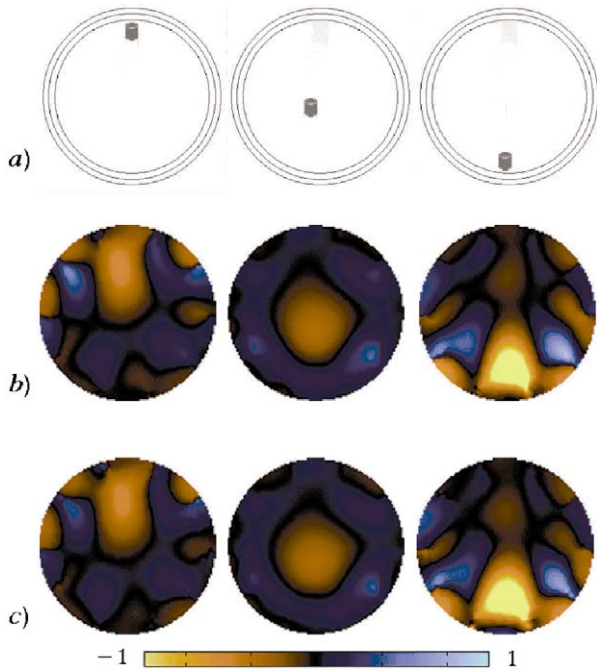


Fig. 6. Images in the transverse plane from the shelled spherical tank data: (a) approximate positions of the Perspex rod, (b) images reconstructed using A_{sphere} , and (c) images reconstructed using $A_{3\text{shell}}$.

Reconstruction of simulated data

No significant differences in localisation accuracy or resolution were evident in the images produced from noiseless simulated data when using either the sensitivity matrix

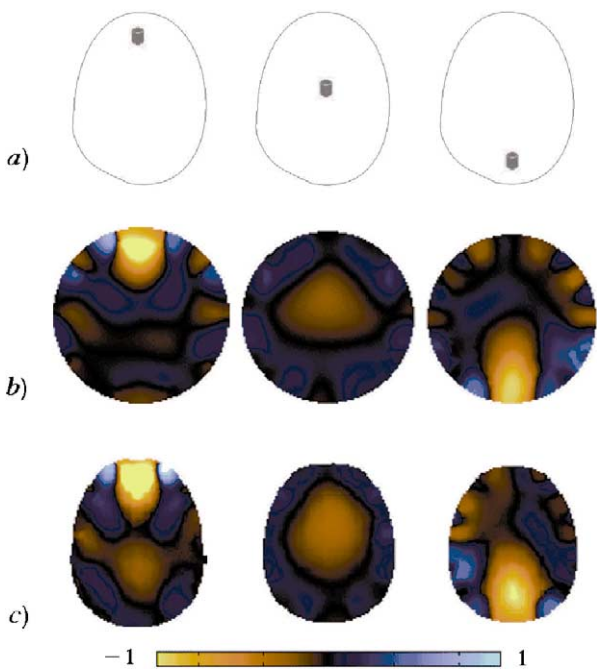


Fig. 7. Images in the transverse plane from the homogeneous head-shaped tank data: (a) approximate positions of the Perspex rod, (b) images reconstructed using A_{sphere} , and (c) images reconstructed using A_{homhead} .

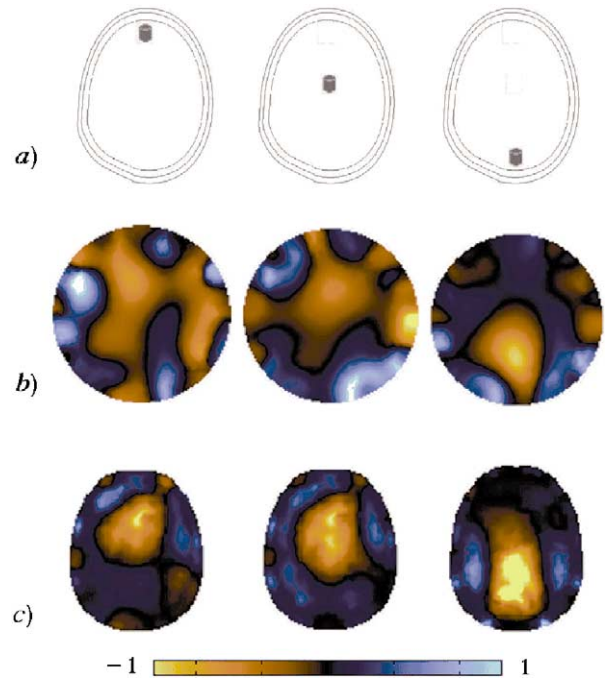


Fig. 8. Images in the transverse plane from data from the head-shaped tank with a skull: (a) approximate positions of the Perspex rod, (b) images reconstructed using A_{sphere} , and (c) images reconstructed using $A_{\text{shellhead}}$.

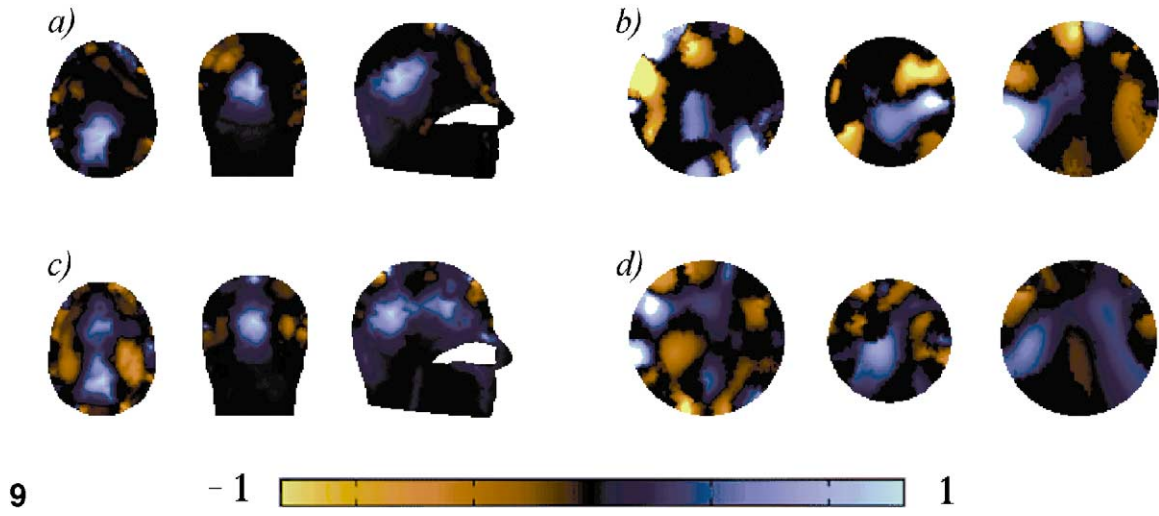
based on an accurate forward model or a homogeneous sphere (Table 2).

Reconstruction of tank data

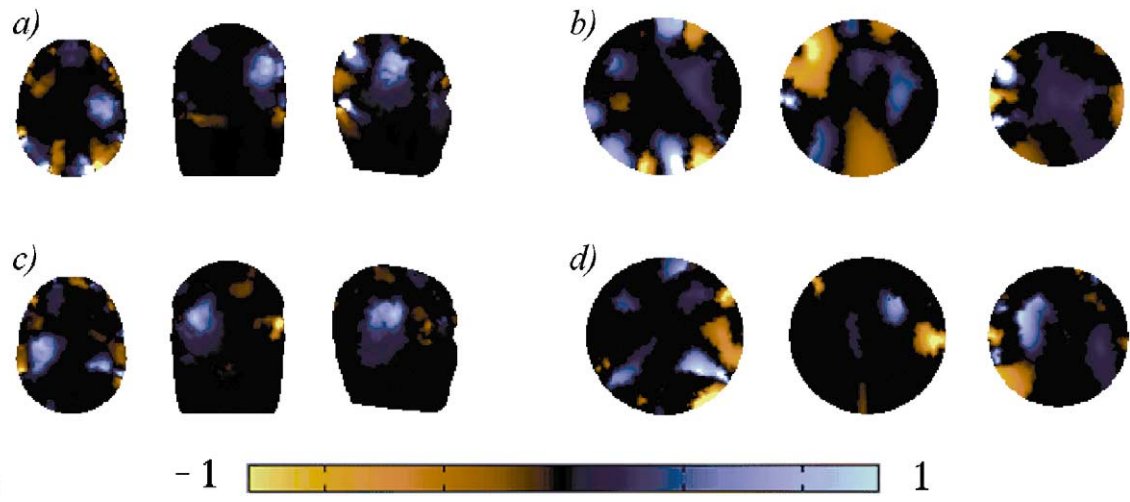
The reconstructions of the data from the spherical tank did not show any significant differences in terms of the localisation accuracy when using the sensitivity matrices based on a three-shell spherical ($A_{3\text{shell}}$) or a homogeneous spherical (A_{sphere}) forward model (Table 2, Fig. 5a and Fig. 6). The resolution when using the more accurate forward model was slightly better ($P = 0.004$, two-tailed paired t test). The mean image quality marks given for the reconstructions based on the more accurate (three shell) forward model were significantly better than those given for the reconstructions based on the homogeneous sphere forward model ($P = 0.00001$, two-tailed paired t test). The observers could not identify which sensitivity matrix was used in the reconstruction process for this data set.

In the images reconstructed from the data collected from the homogeneous head-shaped tank, the sensitivity matrix based on the more accurate forward model (A_{homhead}) led to a slight improvement in the localisation accuracy, particularly in the front of the head ($P = 0.003$, two-tailed paired t test) (Fig. 5b, Fig. 7, and Table 2). There was very little difference in the resolutions measured in the two images sets. The mean image quality marks given for the images produced using A_{homhead} are significantly better than those for the images produced by A_{sphere} ($P = 0.0003$, two-tailed paired t test).

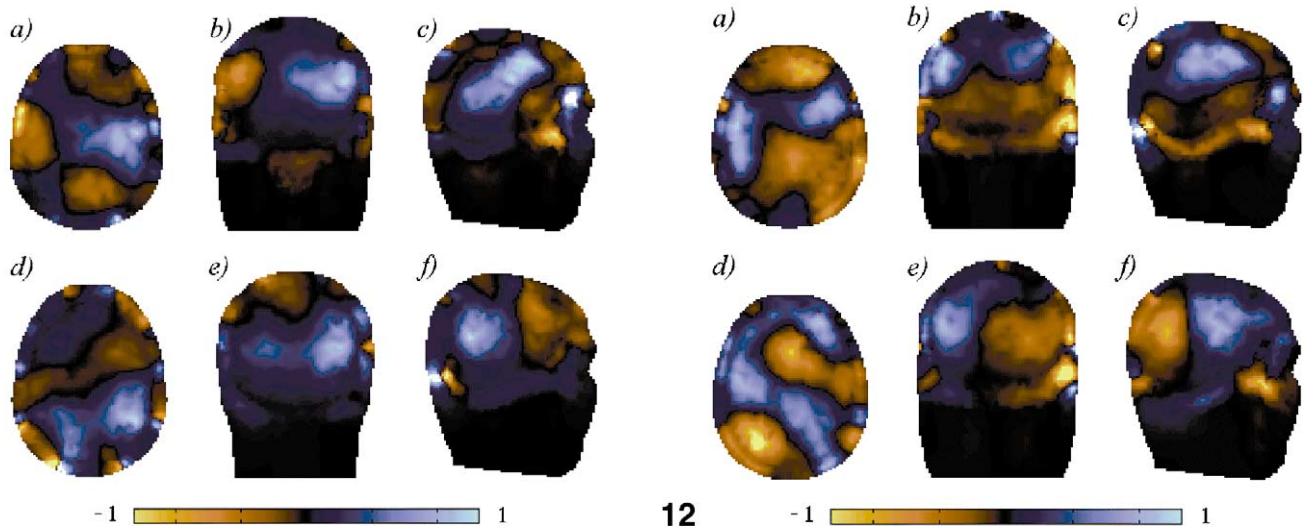
The final set of tank data was collected from the head-



9



10



11

12

Table 2
A summary of the results for simulated, tank and human data

	Localisation error (mm)	HWHM (mm)	Image quality marks
Simulated data			
Four-shell spherical data ($n = 15$)			
Shelled reconstruction	16 ± 7	26 ± 4	x
Homogeneous reconstruction	14 ± 7	27 ± 6	x
Homogeneous head data ($n = 15$)			
Head-shaped reconstruction	21 ± 6	27 ± 8	x
Spherical reconstruction	24 ± 10	28 ± 10	x
Tank data			
Three-shell spherical tank ($n = 11$)			
Shelled reconstruction	15 ± 5	22 ± 5	7.6 ± 0.6 [6–9]
Homogeneous reconstruction	15 ± 5	25 ± 6	6.7 ± 0.6 [6–7]
Homogeneous head tank ($n = 12$)			
Head-shaped reconstruction	13 ± 7	25 ± 8	9.8 ± 0.3 [9–10]
Spherical reconstruction	19 ± 8	26 ± 6	6.1 ± 1.4 [3–8]
Head with Skull Tank ($n = 12$)			
Head-shaped reconstruction	26 ± 8	17 ± 4	4.1 ± 0.8 [2–5]
Spherical reconstruction	24 ± 8	23 ± 3	2.9 ± 1.0 [1–5]
Human data			
Evoked responses ($n = 4$)			
Head-shaped reconstruction	x	x	8.1 ± 1.2 [6–9]
Spherical reconstruction	x	x	2.2 ± 1.0 [1–4]

The mean and standard deviations of the localisation errors and HWHM results for the simulated and tank data. The mean and standard deviation of the quality assessment marks are also given for the tank and the human data, along with the range of the marks in square brackets. The value of n given in brackets for each data set is the number of measurements. An “x” indicates that no data are available.

shaped tank with a human skull (Fig. 5c, Fig. 8, and Table 2). The mean localisation error for the images reconstructed using the sensitivity matrix based on the shelled, head-shaped forward model ($A_{\text{shellhead}}$) was not significantly different from that measured in the images produced using A_{sphere} , although it appears to be somewhat worse in the front of the head. The reconstructed images produced using A_{sphere} failed to produce a localised conductivity change for data containing Perspex at positions of approximately 60 and -10 mm (Fig. 5c). The resolution measured in the images from the sensitivity matrix for the full shelled head was better ($P = 0.0005$, two-tailed paired t test). The t test has been performed only on those positions in which both algorithms produced a localised change. The mean image quality marks given for the images produced using $A_{\text{shellhead}}$ do not differ significantly from those

given for the images produced assuming a homogeneous sphere forward model ($P = 0.03$, two-tailed paired t test).

Reconstruction of human data

a. Visual and motor stimuli

Two examples are shown of images reconstructed from data collected from human volunteers during a visual task (Fig. 9). When using $A_{\text{shellhead}}$, a conductivity increase can be seen toward the rear of the head in each of the three orthogonal planes. The corresponding images produced using A_{sphere} show no consistent localised conductivity increase. The images reconstructed from data collected while the volunteers performed a motor task show similar results

Fig. 9. Two examples of the effect of reconstructing data collected from human volunteers during observation of a 8 Hz chequerboard with $A_{\text{shellhead}}$ (a and c) and A_{sphere} (b and d). The transverse slices shown in a and c are 2 and 8 mm above $z = 0$; the coronal slices are -51 and -57 mm from $y = 0$; and the sagittal slices are 2 and 0 mm from $y = 0$. The same slices are also presented from the images produced using the sensitivity matrix for a homogeneous sphere. Fig. 10. Two examples of the effect of reconstructing data collected from human volunteers performing a motor task with $A_{\text{shellhead}}$ (a and c) and A_{sphere} (b and d). The data reconstructed in a and b are for motor stimulation of the left hand, while those reconstructed in c and d are for motor stimulation of the right hand. The transverse slices shown are 4 mm from $z = 0$; the coronal slices are -7 and -10 mm from $y = 0$; and the sagittal slices are 48 and -42 mm from $y = 0$.

Fig. 11. Reconstructions of data collected approximately 6 s prior to the electrographic onset of two right temporal complex partial seizures in patient 1. Slices a–c are reconstructed from data collected during one seizure, slices d–f are reconstructed from data collected during another seizure. In both cases, three orthogonal planes are shown through the maximum conductivity increase. The transverse slices a and d are 8 and 21 mm, respectively, above the $z = 0$ plane; the coronal slices b and e are -44 and -61 mm, respectively, from $y = 0$; and the sagittal slices c and f are 57 and 44 mm, respectively, from $x = 0$.

Fig. 12. Reconstructions of data collected approximately 10 s after the electrographic onset of two left temporal complex partial seizures in patient 2. Slices a–c are reconstructed from data collected during one seizure, slices d–f are reconstructed from data collected during another seizure. In both cases, three orthogonal planes are shown through the maximum conductivity increase. The transverse slices a and d are 23 and 19 mm, respectively, above the $z = 0$ plane; the coronal slices b and e are both -3 mm from $y = 0$; and the sagittal slices c and f are both -46 mm from $x = 0$.

(Fig. 10), with much clearer localisation of a conductivity increase in the images reconstructed using $A_{\text{shellhead}}$. The mean marks given in the image quality assessment for the visual and motor stimuli images were significantly better when the more accurate forward model was used in the reconstruction process ($P = 0.004$, two-tailed paired t test, Table 2).

b. Ictal

The images reconstructed from data collected ictally show conductivity increases in the appropriate hemisphere of the brain. In patient 1 (Fig. 11) the conductivity increase was in the right temporal region, while in patient 2 it was in the left temporal region (Fig. 12).

Discussion

A reconstruction algorithm based on the finite element method which incorporates realistic geometry and conductivities in the forward model has been presented, and the effect on reconstructed images has been assessed using simulated data, data collected from tank phantoms, and data collected from human volunteers. Significant differences existed when comparing images reconstructed assuming an accurate forward model and a homogeneous sphere forward model. In general, the results using the more accurate forward models were better, although it is perhaps surprising that more significant gains in localisation accuracy and resolution have not been noted when using a more accurate forward model. Preliminary work using data collected from human volunteers suggests that the most significant benefits of using a more accurate forward model will be apparent when attempting functional imaging of the human brain.

Technical considerations

The comparison of the forward voltages in the homogeneous case demonstrates a similar level of agreement between the numerical and the analytical solutions to that which has been reported for other three-dimensional implementations of the finite element method (Thevenet et al., 1991; Marin et al., 1998). This confirms the accuracy of the FEM implementation. Further improvements to the accuracy of the modelling are likely to be gained by implementing a number of refinements to the method. The use of linear finite elements will lead to errors in regions where the electric field is changing very rapidly, particularly in the scalp, skull, and CSF which in the current meshes have only one or two layers of linear finite elements across them. Incorporating higher order finite elements will help model the electric field in these layers more accurately while minimising the extra number of elements needed in the mesh (Awada et al., 1997). In addition, selectively increasing the mesh density beneath the electrodes (Molinari et al., 2001) and incorporating a realistic electrode model (Vauhkonen,

1997) will help to reduce the artificially high current density calculated at the electrodes and may reduce artefacts in the images. The accuracy of the forward solution for the realistic head is likely to be improved by addressing these issues.

Improvements in the accuracy of the reconstructed images are likely to be gained by optimising the way in which the sensitivity matrices are normalised and the singular value at which they are truncated upon inversion. The methods that have been adopted in the current work are acceptable for comparisons between sensitivity matrices based on two alternative forward models, but are not optimised on an individual basis for each sensitivity matrix. In addition, alternative methods of inverting the sensitivity matrices, such as using a nonlinear iterative inversion which optimises the fit between the measured voltages and the voltages generated from a successively updated conductivity distribution, may lead to improvements in the images (e.g., Edic et al., 1998).

Summary of simulated data and phantom studies

Two of the questions that this work was intended to address concerned the effect of incorporating realistic geometry and inhomogeneous conductivity distributions into the forward model. The results suggest that incorporating realistic conductivity distributions in the forward model can improve the resolution and quality of the images, compared with using a homogeneous forward model. Similarly, using realistic geometry in the forward model leads to a slight improvement in the localisation accuracy and the image quality. The improvements in image quality found when using a more accurate forward model were more significant than the effects on the localisation accuracy or the resolution.

The results from the head-shaped tank with a skull are inconclusive, although it is interesting that when using the sensitivity matrix based on the homogeneous sphere forward model, there was a failure to produce a clear localised change in two positions. This is relevant when considering the results from the human data, particularly since an insulator was introduced into the tank phantoms whereas conductivity changes of less than 20% are expected in the brain. Of all of the “correct” forward models used in the tank studies, the full shelled head is the least ideal, since it has conductivities appropriate to the human head rather than the tank itself. The resistivity ratio of 98:1 between the skull and brain region in the head-shaped tank (Tidswell et al., 2001b) is considerably higher than that assumed in the forward model, and may be responsible for the relatively poor localisation in the front of the head when using the sensitivity matrix based on the full shelled head forward model. Further work is necessary to determine what effect uncertainty in the conductivity values has on the images.

Summary of results using data from human volunteers

Using the sensitivity matrix calculated assuming the full shelled head forward model to reconstruct data from human volunteers produces clear benefits, particularly in terms of the subjective image quality. In the examples shown, which were chosen on the basis that a conductivity increase, corresponding to a blood volume increase, was apparent with reasonable localisation when using the realistic forward model, there is a clear improvement. This is often to the extent that there is no obviously dominant localised conductivity change when reconstructing the same data using the sensitivity matrix for the homogeneous sphere. At this stage, it is not clear whether this is a general result and how many extra positive results might be expected if the more accurate forward model was used. Work is currently ongoing to reanalyse the data presented by Tidswell et al. (2001a) to see whether the use of the sensitivity matrix for the full shelled head can lead to a higher percentage of images with correctly localised conductivity changes. One of the main questions in that work was whether the localisation errors were the result of the approximations made in the forward model of the reconstruction algorithm or whether they were due to the physiological mechanisms underlying the conductivity changes in the brain during functional activity. The current study suggests that a large proportion of the error was due to the reconstruction algorithm. There remain substantial areas of activation, both conductivity increases and decreases, which may correspond to the increases and decreases in blood volume that are observed in functional PET and SPECT experiments (see, for example, Mentis et al., 1997; Catalan et al., 1998). Further improvements in the accuracy of the forward model will continue to provide information on this subject. One definite advantage of the shelled head is that artefacts which arise as a result of errors in the positioning of the electrodes tend to be confined to the scalp and skull layers of the images, leaving the brain region much clearer.

The preliminary results presented from the data that have been collected ictally are encouraging, although no substantial claims can be made for them at this stage. In the two subjects considered, localised conductivity increases can be seen with the same lateralisation as is expected from the EEG telemetry data. In addition, the images produced from two seizures in the same patient are consistent with each other. This study is currently ongoing, but the preliminary findings in this paper encourage the idea that EIT may be able to offer functional imaging in ambulant patients undergoing presurgical EEG telemetry, which would provide a valuable addition to current clinical practice.

Acknowledgments

We thank Professor Simon Arridge and Dr. Martin Schweiger of the Department of Computer Science, UCL,

for the use of TOAST. This work was supported by the Epilepsy Research Foundation (A.P.B. and M.K.S.), the Engineering and Physical Sciences Research Council (A.P.B.), and the Medical Research Council (A.T.T.).

References

- Awada, K.A., Jackson, D.R., Williams, J.T., Wilton, D.R., Baumann, S.B., Papanicolaou, A.C., 1997. Computational aspects of finite element modelling in EEG source localisation. *IEEE Trans. Biomed. Eng.* 44, 736–752.
- Barber, D.C., Seagar, A.D., 1987. Fast reconstruction of resistance images. *Clin. Phys. Physiol. Meas.* 10, 368–370.
- Baumann, S.B., Wozny, D.R., Kelly, S.K., Meno, F.M., 1997. The electrical conductivity of human cerebrospinal fluid at body temperature. *IEEE Trans. Biomed. Eng.* 44, 220–223.
- Bayford, R.H., Gibson, A., Tizzard, A., Tidswell, A.T., Holder, D.S., 2001. Solving the forward problem in electrical impedance tomography for the human head using I-DEAS (integrated design engineering analysis software), a finite element modelling tool. *Physiol. Meas.* 22, 55–64.
- Binnie, C.D., Rowan, A.J., Gutter, T., 1982. *A Manual of Electroencephalographic Technology*. Cambridge Univ. Press, UK.
- Bonovas, P.M., Kyriacou, G.A., Sahalos, J.N., 2001. A realistic three dimensional FEM of the human head. *Physiol. Meas.* 22, 65–76.
- Boone, K., Barber, D.C., Brown, B.H., 1997. Imaging with electricity: report of the European Concerted Action on impedance tomography. *J. Med. Eng. Technol.* 21, 201–232.
- Burger, H.C., Milaan, J.B.V., 1943. Measurements of the specific resistance of the human body to direct current. *Acta Med. Scand.* 114, 584–607.
- Burnett, D.S., 1987. *Finite Element Analysis: From Concepts to Applications*. Addison-Wesley, UK.
- Catalan, M.J., Honda, M., Weeks, R.A., Cohen, L.G., Hallett, M., 1998. The functional neuroanatomy of simple and complex sequential finger movements: a PET study. *Brain* 121, 253–264.
- Crouzeix, A., Yvert, B., Bertrand, O., Pernier, J., 1999. An evaluation of dipole reconstruction accuracy with spherical and realistic head models in MEG. *Clin. Neurophysiol.* 110, 2176–2188.
- Cherepenin, V., Karpov, A., Korjenskyy, A., Kornienko, V., Mazaletskaya, A., Mazourov, D., Meister, D., 2001. A 3D electrical impedance tomography (EIT) system for breast cancer detection. *Physiol. Meas.* 22, 9–18.
- Cuffin, B.N., 2001. Effects of modelling errors and EEG measurement montage on source localisation accuracy. *J. Clin. Neurophys.* 18, 37–44.
- Cuffin, B.N., Schomer, D.L., Ives, J.R., Blume, H., 2001. Experimental tests of EEG source localisation accuracy in spherical head models. *Clin. Neurophysiol.* 112, 46–51.
- Dehghani, H., 1999. *Finite element modelling and image reconstruction in single and multi-frequency electrical impedance tomography*. Ph.D. thesis. Sheffield Hallam Univ., UK.
- Edic, P.M., Isaacson, D., Saulnier, G.J., Jain, H., Newell, J.C., 1998. An iterative Newton-Raphson method to solve the inverse admittivity problem. *IEEE Trans. Biomed. Eng.* 45, 899–908.
- Geddes, L.A., Baker, L.E., 1967. The specific resistance of biological material—a compendium of data for the biomedical engineer and physiologist. *Med. Biol. Eng.* 5, 271–293.
- Geselowitz, D.B., 1971. An application of electrocardiographic lead theory to impedance plethysmography. *IEEE Trans. Biomed. Eng.* 18, 38–41.
- Gibson, A., 2000. *Electrical impedance tomography of human brain function*. Ph.D. thesis. University College London, UK.
- Gibson, A., Bayford, R.H., Holder, D.S., 2000. Two dimensional finite element modelling of the neonatal head. *Physiol. Meas.* 21, 45–52.
- Golub, G.H., Loam, C.F.V., 1996. *Matrix Computations*. John Hopkins Univ. Press, Baltimore, MD.

- Hansen, P.C., 1998. Analysis of discrete ill-posed problems by means of the L-curve. *SIAM Rev.* 34, 561–580.
- Harris, N.D., Suggestt, A.J., Brown, B.H., Barber, D.C., 1988. Applied potential tomography: a new technique for monitoring pulmonary function. *Clin. Phys. Physiol. Meas.* 9, 79–86.
- Holder, D.S., Rao, A., Hanquan, Y., 1996. Imaging of physiologically evoked responses by electrical impedance tomography with cortical electrodes in the anaesthetised rabbit. *Physiol. Meas.* 17, A179–A186.
- Huiskamp, G., Vroeijsstijn, M., van Dijk, R., Wieneke, G., van Huffelen, A.C., 1999. The need for correct realistic geometry in the inverse EEG problem. *IEEE Trans. Biomed. Eng.* 46, 1281–1287.
- Jain, H., Isaacson, D., Edic, P.M., Newell, J.C., 1997. Electrical impedance tomography of complex conductivity distributions with noncircular boundary. *IEEE Trans. Biomed. Eng.* 44, 1051–1060.
- Jin, J.-M., 1993. *The Finite Element Method in Electromagnetics*. Wiley, New York.
- Kevorkian, J., 1990. *Partial Differential Equations: Analytical Solution Techniques*. Wadsworth and Brookes/Cole, Belmont, CA.
- Kleinermann, F., 2001. Three dimensional modelling of electrical impedance tomography. Ph.D. thesis. Univ. of Salford, UK.
- Kotre, C.J., 1994. EIT image reconstruction using sensitivity weighted filtered back projection. *Physiol. Meas.* 15, 125–136.
- Law, S.K., 1993. Thickness and resistivity variations over the surface of the human skull. *Brain Topography* 6, 99–109.
- Lux, H., Heinemann, U., Dietzel, I., 1986. Ionic changes and alterations in the size of the extracellular space during epileptic activity. *Adv. Neurol.* 44, 619–639.
- Mangall, Y., Baxter, A., Avill, A., Bird, N., Brown, B., Barber, D., Seager, A., Johnson, A., Read, N., 1987. Applied potential tomography: a new noninvasive technique for assessing gastric function. *Clin. Phys. Physiol. Meas.* 8, 119–129.
- Marin, G., Guerin, C., Baillet, S., Garnero, L., Meunier, G., 1998. Influence of skull anisotropy for the forward and inverse problem in EEG: simulation studies using FEM on realistic head models. *Hum. Brain Mapp.* 6, 250–269.
- Menninghaus, E., Lütkenhöner, B., Gonzalez, S.L., 1994. Localisation of a dipolar source in a skull phantom: realistic versus spherical model. *IEEE Trans. Biomed. Eng.* 41, 986–989.
- Mentis, M.J., Alexander, G.E., Grady, C.L., Horowitz, B., Krasuski, J., Pietrini, P., Strassburger, T., Hampel, H., Schapiro, M.B., Rappoport, S.I., 1997. Frequency variation of a pattern-flash visual stimulus during PET differentially activates brain from striate through frontal cortex. *NeuroImage* 5, 116–128.
- Metherall, P., Barber, D.C., Smallwood, R.H., Brown, B.H., 1996. Three dimensional electrical impedance tomography. *Nature* 380, 509–512.
- Molinari, M., Cox, S.J., Blott, B.H., Daniell, G.J., 2001. Adaptive mesh refinement for electrical impedance tomography. *Physiol. Meas.* 22, 91–96.
- Murai, T., Kagawa, Y., 1985. Electrical impedance computed tomography based on a finite element model. *IEEE Trans. Biomed. Eng.* 32, 177–184.
- Oostendorp, T.F., Delbeke, J., Stegeman, G.F., 2000. The conductivity of the human skull: results of in vivo and in vitro measurements. *IEEE Trans. Biomed. Eng.* 47, 1487–1492.
- Osterman, K.S., Kerner, T.E., Williams, D.B., Hartov, A., Poplack, S.P., Paulsen, K.D., 2000. Multifrequency electrical impedance imaging: preliminary in vivo experience in the breast. *Physiol. Meas.* 21, 99–110.
- Rao, A., 2000. *Electrical impedance tomography of brain activity: studies into its accuracy and physiological mechanisms*. Ph.D. thesis. Univ. College London, UK.
- Roth, B.J., Balish, M., Gorbach, A., Sato, S., 1993. How well does a three-sphere model predict positions of dipoles in a realistically shaped head? *Electroenceph. Clin. Neurophysiol.* 87, 175–184.
- Saha, S., Williams, P.A., 1992. Electric and dielectric properties of wet human cortical bone as a function of frequency. *IEEE Trans. Biomed. Eng.* 39, 1298–1304.
- Serrano, R.E., de Lema, B., Casas, O., Feixzs, T., Calaf, N., Camacho, V., Carrio, I., Casan, P., Sanchis, J., Riu, P.J., 2002. Use of electrical impedance tomography (EIT) for the assessment of unilateral pulmonary function. *Physiol. Meas.* 23, 211–220.
- Tarassenko, L., 1985. *Electrical impedance techniques for the study of the cerebral circulation and cranial imaging in the newborn*. Ph.D. thesis. Oxford Univ, UK.
- Thevenet, M., Bertrand, O., Perrin, F., Dumont, T., Pernier, J., 1991. The finite element method for a realistic head model of brain activities: preliminary results. *Clin. Phys. Physiol. Meas.* 12, 89–94.
- Tidswell, A.T., Gibson, A., Bayford, R.H., Holder, D.S., 2001a. Three dimensional electrical impedance tomography of human brain activity. *NeuroImage* 13, 283–294.
- Tidswell, A.T., Gibson, A., Bayford, R.H., Holder, D.S., 2001b. Validation of a 3D reconstruction algorithm for EIT of human brain function in a realistic head-shaped tank. *Physiol. Meas.* 22, 177–185.
- Tidswell, A.T., Gibson, A., Bayford, R.H., Holder, D.S., 2001c. Electrical impedance tomography of human brain activity with a two-dimensional ring of scalp electrodes. *Physiol. Meas.* 22, 167–175.
- Towers, C.M., McCann, H., Wang, M., Beatty, P.C., Pomfrett, C.J.D., Beck, M.S., 2000. 3D simulation of EIT for monitoring impedance variations within the human head. *Physiol. Meas.* 21, 119–124.
- van den Broek, S.P., Reinders, F., Donderwinkel, M., Peters, M.J., 1998. Volume conduction effects in EEG and MEG. *Electroenceph. Clin. Neurophysiol.* 106, 522–534.
- Vauhkonen, M., 1997. *Electrical impedance tomography and prior information*. Ph.D. thesis. Univ. of Kuopio, Finland.
- Webster, J.G., 1990. *Electrical Impedance Tomography*. IOP Publishing, UK.
- Weinand, M.E., Carter, L.P., El-Saadany, W.F., Sioutos, P.J., Labiner, D.M., Oommen, K.J., 1997. Cerebral blood flow and temporal lobe epileptogenicity. *J. Neurosurg.* 86, 226–232.
- Xu, P., 1998. Truncated, SVD methods for discrete linear ill-posed problems. *Geophys. J. Int.* 135, 505–514.
- Yerworth, R.J., Bayford, R.H., Cusick, G., Conway, M., Holder, D.S., 2002. Design and performance of the UCLH Mark 1b 64 channel electrical impedance tomography (EIT) system, optimised for imaging human brain function. *Physiol. Meas.* 23, 149–158.
- Yvert, B., Bertrand, O., Thévenet, M., Echallier, J.F., Pernier, J., 1997. A systematic evaluation of the spherical model accuracy in EEG dipole localisation. *Electroenceph. Clin. Neurophysiol.* 102, 452–459.
- Zahdakoochak, M., Blott, B.H., Hames, T.K., George, R.F., 1991. Spectral expansion analysis in electrical impedance tomography. *J. Phys. D* 24, 1911–1916.